

# Anomalous, non-Gaussian tracer diffusion in heterogeneously crowded environments

Surya K. Ghosh<sup>†,‡</sup>, Andrey G. Cherstvy<sup>†</sup>, Denis S. Grebenkov<sup>‡</sup>,  
and Ralf Metzler<sup>†,‡,1</sup>

<sup>†</sup> Institute for Physics & Astronomy, University of Potsdam, 14476 Potsdam-Golm, Germany

<sup>‡</sup> Physics of Condensed Matter, CNRS École Polytechnique, 91128 Palaiseau, France

<sup>‡</sup> Department of Physics, Tampere University of Technology, 33101 Tampere, Finland

E-mail: <sup>1</sup>rmetzler@uni-potsdam.de

**Abstract.** A topic of intense current investigation pursues the question how the highly crowded environment of biological cells affects the dynamic properties of passively diffusing particles. Motivated by recent experiments we report results of extensive simulations of the motion of a finite sized tracer particle in a heterogeneously crowded environment. For given spatial distributions of monodisperse crowders we demonstrate how anomalous diffusion with strongly non-Gaussian features arises in this model system. We investigate both biologically relevant situations of particles released either at the surface of an inner domain (*nucleus*), or at the outer boundary (*cell membrane*), exhibiting distinctly different behaviour of the observed anomalous diffusion for heterogeneous crowder distributions. Specifically we reveal an extremely asymmetric spreading of the tracer even at moderate crowding fractions. In addition to the standard mean squared displacement and the local diffusion exponent of the tracer particles we investigate the magnitude and the amplitude scatter of the time averaged mean squared displacement of individual trajectories, the non-Gaussianity parameter, and the van Hove correlation function of the particle displacements. We also quantify how the average tracer diffusivity varies with the position in the domain with heterogeneous radial distribution of the crowders and examine the behaviour of the survival probability and the dynamics of first passage events of the tracer. Finally, we discuss the relevance of our results to single particle tracking measurements in biological cells.

## 1. Introduction

The cytoplasmic fluid of living cells is a supercrowded medium [1], in which biomacromolecules occupy volume fractions reaching 30% and higher [2, 3, 4, 5, 6]. This macromolecular crowding (MMC) affects the diffusion of larger passive molecules, endogenous as well as artificially introduced submicron tracer particles, and cellular components [7]. One of the central observations is the existence of transient but often very extended anomalous diffusion [8, 9] with the sublinear scaling

$$\langle \mathbf{r}^2(t) \rangle \simeq K_\beta t^\beta \tag{1}$$

of the mean squared displacement (MSD) of the diffusing particles with the anomalous diffusion exponent in the subdiffusive range  $0 < \beta < 1$  [7, 10]. Here  $K_\beta$  is the generalised diffusion coefficient with units  $\text{cm}^2/\text{sec}^\beta$ . Subdiffusion in the crowded cytoplasm of living cells was observed for fluorescently labelled and autofluorescent small proteins [11, 12], labelled polymeric dextrane [13] and messenger RNA [1, 14], chromosomal loci and telomeres [14, 15], as well as submicron endogenous granules [16, 17, 18] and viruses [19]. Subdiffusion was also reported for the motion of tracer particles in artificially crowded environments [20, 21, 22, 23, 24, 25, 26, 27, 28], and it also occurs in cell membranes, as shown experimentally [29, 30, 31] and by molecular dynamics as well as coarse grained simulations [32, 33, 34, 35]. In addition, active transport processes in living cells may lead to superdiffusion with  $1 < \beta < 2$  [36, 37, 38, 39].

Particle diffusion in crowded and structured environments has been in the focus of a number of computer simulations [40, 41, 42, 43, 44, 45] and theoretical studies [7, 41, 46, 47]. The observed anomalous diffusion in such systems is addressed by various generalised stochastic processes, as summarised in references [48, 49, 50]. Specifically in an environment of densely packed, freely moving crowders the tracer diffusion was demonstrated to follow Brownian motion at sufficiently long times [44], whereas for crowders confined by a potential and for static crowders the tracer diffusion features a very extended albeit ultimately transient subdiffusive regime [44, 54].

The current study is motivated by recent experimental evidence of an inherently polydisperse mixture of crowding proteins in both the bacterial and eukaryotic cytoplasm [6, 44, 45]. Moreover, the distribution of crowders in the cell was shown to be rather heterogeneous, giving rise to a faster particle mobility of small tracer proteins near the cell nucleus of surface-adhered eukaryotic cells [55], see also the heterogeneous diffusivity map in reference [56]. These properties of the cell cytoplasm impose severe restrictions on the rates of biochemical reactions [57, 58] including those involving polymer dynamics [59, 60, 61, 62] and often impair the diffusion of particles inside cells [44, 45, 54].

Here we address two aspects of crowding, a finite size of the tracer and a heterogeneous distribution of crowders in a two dimensional, circular model cell with a central nucleus region. In the space between the outer cell boundary and the inner nucleus we place either homogeneously or heterogeneously distributed monodisperse crowders, and then simulate the motion of a finite sized tracer particle through this static crowder configuration. We investigate the two biologically relevant scenarios of in-out (from nucleus to cell boundary) versus out-in (from cell boundary to nucleus) tracer diffusion, finding fundamental differences in the observed dynamics. From extensive simulations we determine the particle distribution for different crowding environments and study the particle dynamics in terms of the ensemble and time averaged MSDs. We further analyse the non-Gaussianity of particle trajectories, the van Hove position correlation function, as well as the first passage statistics of the tracer.

The paper is organised as follows. In the next section we set up the model, discuss the simulation procedure and the data analysis. In sections 3 and 4 we describe the main

results for the homogeneous and heterogeneous cases, respectively, and compare them to theoretical models. Further analyses of both cases in terms of the non-Gaussianity parameter and the van Hove correlation function are presented in section 5 while the first passage statistics are discussed in section 6. In section 7 we draw our conclusions and discuss some applications of our results.

## 2. Model, simulations scheme, and data analysis

We consider a model cell in the form of a planar circular annulus between the nucleus, represented by the excluded region within the radius  $a$ , and the plasma membrane located at radius  $R$ , as shown in figure 1. The space between the membrane and the nucleus is filled with *static* monodisperse crowders of radius  $R_c$ . We consider two cases: homogeneous distribution of crowders with a prescribed crowding (area) fraction  $\phi$ , and heterogeneous distribution of crowders with a linear radial gradient

$$\phi(r) = \phi(a) + \frac{\phi(R) - \phi(a)}{R - a}(r - a) \quad (2)$$

for  $a < r < R$ . For most cases we set  $\phi(a) = 0.01$  and  $\phi(R) \approx 0.3$ . As we show below, equation (2) leads to a transiently subdiffusive tracer motion from the nucleus to the cell membrane, emerging due to an increasing density of crowders near the cell periphery, as evidenced by figure 1, panels C and D.

In the simulations the crowders are placed at random positions without overlap. The highest crowding fraction we simulated was around 30%. When computing the mean time averaged MSD in equation (7) below, we typically average over  $M = 10^2$  random configurations of crowders. This disorder average is taken in addition to the average over individual trajectories in a given, quenched crowder configuration. The tracer particle has a fixed unit radius. We set the radius of the circular membrane to  $R = 100$  and the radius of the inner nucleus to  $a = 30$ , so that the ratio  $a/R$  is similar to that of a typical eukaryotic cell [55]. The radii in the simulations and in the plots are measured in terms of the length scale  $\sigma$  of the potential (3).

The Weeks-Chandler-Andersen repulsive potential given by the 6-12 Lennard-Jones potential  $E_{\text{LJ}}(r)$  with the standard cutoff distance  $r_{\text{cut}}$  is used to parameterise the repulsion between the tracer and crowders,

$$E_{\text{LJ}}(r) = 4\epsilon \left[ \left( \frac{\sigma}{r} \right)^{12} - \left( \frac{\sigma}{r} \right)^6 + \frac{1}{4} \right] \quad (3)$$

for  $r < r_{\text{cut}} = 2^{1/6}\sigma$ , and  $E_{\text{LJ}}(r) = 0$  otherwise [63]. We simulate the dynamics of the centre position  $\mathbf{r}(t)$  of the tracer via the Langevin equation

$$m \frac{d^2 \mathbf{r}(t)}{dt^2} = - \sum_J \nabla \left[ E_{\text{LJ}}(|\mathbf{r} - \mathbf{R}_J| - (R_c + \sigma)) + E_{\text{LJ}}(|\mathbf{r}| - (a + \sigma)) \right. \\ \left. + E_{\text{LJ}}((R - \sigma) - |\mathbf{r}|) \right] - \xi \mathbf{v}(t) + \mathbf{F}(t), \quad (4)$$

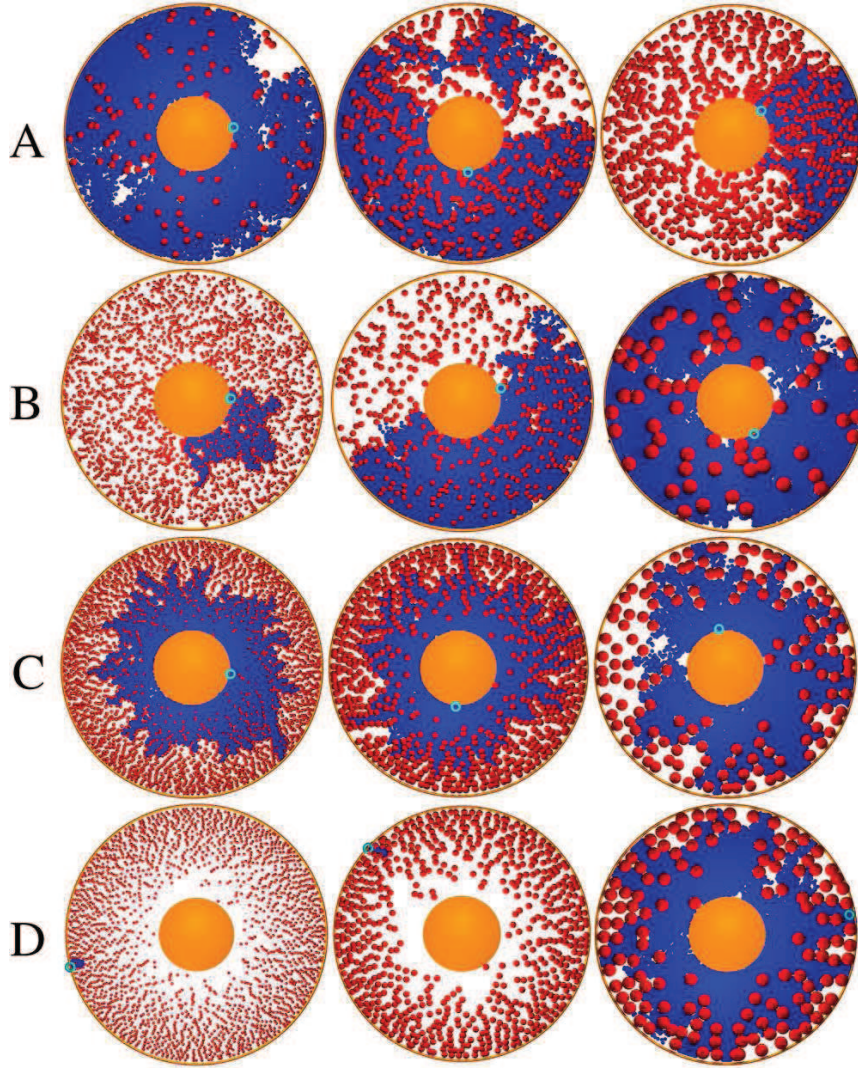


**Figure 1.** Diffusion profiles for homogeneously (panels A and B) and heterogeneously (panels C and D) distributed monodisperse crowders. In panel A the fraction of crowders increases from left to right:  $\phi = 0.05, 0.2, 0.3$ , and the size of the crowders is fixed to  $R_c = 2$ . In panel B the size of the crowders grows from left to right:  $R_c = 1, 2, 5$ , while the crowding fraction is fixed at  $\phi = 0.2$ . For heterogeneous crowders distributions in panels C and D, the crowding fraction  $\phi(r)$  exhibits the linear growth (2) in radial direction. The cell nucleus is represented by the excluded disk at the centre, shown in orange. The diffusion is in-out (i.e., from the nucleus to the membrane) in panel C and out-in (from the membrane to the nucleus) in panel D. The initial tracer position is shown by the small blue circle. The crowder radius in panels C and D grows from left to right:  $R_c = 1, 2, 5$ . The regions of the domain visited by the tracer up to the diffusion time  $T = 10^4$  are depicted in blue. Major asymmetries arise at higher crowding fraction and in heterogeneous systems.

where  $m$  is the mass of the tracer particle,  $\xi$  is the friction coefficient experienced by the tracer particle,  $\mathbf{v}(t)$  is its velocity, and  $\mathbf{R}_J$  is the static position of the  $J$ th crowder. Finally  $\mathbf{F}(t)$  represents a Gaussian  $\delta$  correlated noise with zero mean and covariance

$$\langle \mathbf{F}_j(t) \cdot \mathbf{F}_k(t') \rangle = 2\delta_{j,k}\xi k_B \mathcal{T} \delta(t - t'). \quad (5)$$

The inertial term in equation (4) gives rise to a ballistic regime in the particle dynamics, as shown below (see reference [54] for more details on this regime). In the simulations below we set  $\epsilon = k_B \mathcal{T} = 1$ ,  $m = 1$ , and  $\xi = 1$  corresponding to moderate damping [64, 65, 66]. At these scales, the diffusivity of a tracer in an uncrowded environment is  $D_0 = k_B \mathcal{T} / \xi = 1$ . The unit time step of simulations corresponds to the physical time  $\tau = \sigma \sqrt{m / (k_B \mathcal{T})}$ . We employ the Verlet velocity algorithm with the time step  $\delta t = 0.01$  to integrate the stochastic equation (4).

To characterise the diffusion behaviour we evaluate the time averaged MSD

$$\overline{\delta^2(\Delta)} = \frac{1}{T - \Delta} \int_0^{T - \Delta} [\mathbf{r}(t + \Delta) - \mathbf{r}(t)]^2 dt \quad (6)$$

for individual particle trajectories  $\mathbf{r}(t)$ . Here  $T$  is the length of the trajectory (observation time) and  $\Delta$  is the lag time defining the width of the window slid along the trajectory. This definition of the time average is standard in single particle tracking experiments [1, 10, 50, 67]. For  $N$  individual trajectories the ensemble average is approximated as

$$\langle \overline{\delta^2(\Delta)} \rangle = \frac{1}{N} \sum_{i=1}^N \overline{\delta_i^2(\Delta)}. \quad (7)$$

In the scenario of quenched heterogeneous environments considered herein we also calculate the disorder average of the time averaged MSD over  $M$  different realisations of the crowding environment (compare [68, 69])

$$\langle \widetilde{\overline{\delta^2(\Delta)}} \rangle = \frac{1}{M} \sum_{j=1}^M \langle \overline{\delta^2(\Delta)} \rangle_j. \quad (8)$$

The ensemble averaged MSD is also computed as double average over  $N$  tracer trajectories for each crowders distribution and  $M$  crowders distributions:

$$\langle \mathbf{r}^2(t) \rangle = \langle [\widetilde{\mathbf{r}(t) - \mathbf{r}(0)}]^2 \rangle = \frac{1}{MN} \sum_{j=1}^M \sum_{i=1}^N [\mathbf{r}_i(t) - \mathbf{r}_i(0)]_j^2. \quad (9)$$

### 3. Homogeneous crowding case: ensemble and time averaged mean squared displacements

We start with the analysis of the tracer diffusion among static homogeneously distributed crowders as shown in figure 1 in panels A and B. Figure 2 shows the ensemble averaged MSD  $\langle \mathbf{r}^2(t) \rangle$  and the corresponding local MSD scaling exponent

$$\beta = \frac{d \log \langle \mathbf{r}^2(t) \rangle}{d \log t}. \quad (10)$$

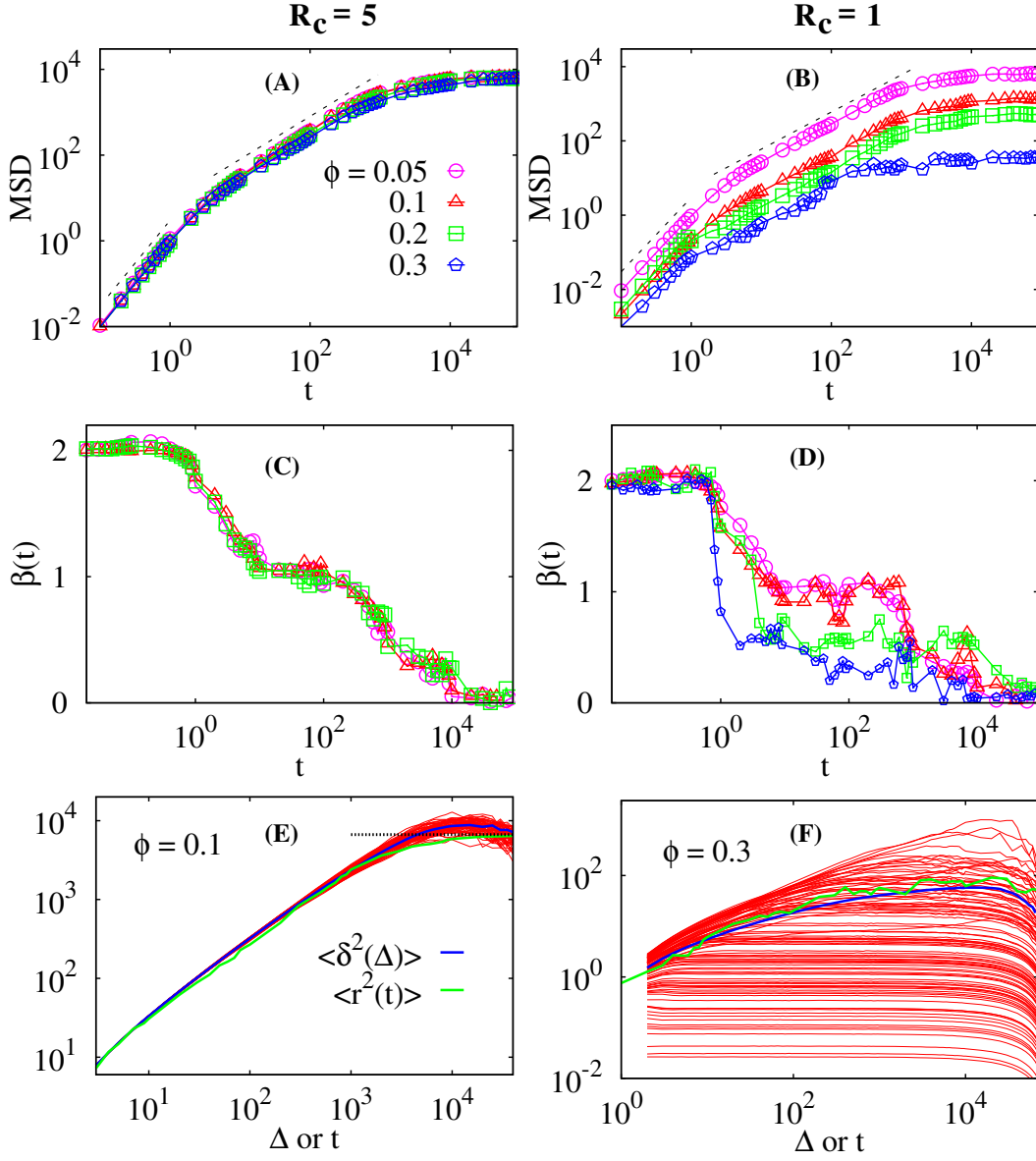


**Figure 2.** MSD, local scaling exponent  $\beta(t)$ , and time averaged MSD  $\langle \overline{\delta^2} \rangle$  for tracer diffusion in an environment of homogeneously distributed crowders. The two columns correspond to different crowder radii:  $R_c = 5$  (left) and  $R_c = 1$  (right). The data for different crowding fractions  $\phi$  are shown by different symbols in the panels A, B, C, and D. In panels A and B the two dashed lines indicate the ballistic asymptote at short times and the linear Brownian growth at intermediate times. In panels E and F 100 individual time averaged MSD curves for a particular distribution of crowders are plotted. In panel E the long time plateau (11) of the MSD is shown by the dotted line. Parameters: the radius of the domain is  $R = 100$  and the radius of the excluded nucleus region is  $a = 30$ . The crowding fraction  $\phi$  is indicated in the panels. Where applicable, the number of different crowders configurations used in the averaging for the MSD and the scaling exponent is  $M = 100$  (disorder averaging), the number of tracer trajectories in each crowders configuration is  $N = 100$  so that the total number of tracers used for averaging is  $M \times N = 10^4$ .

Both the crowding fraction  $\phi$  and the crowder radius  $R_c$  are varied.

For relatively large crowders an initial ballistic growth of the MSD (corresponding to underdamped particle motion, see also [54]) crosses over to a quite prolonged Brownian regime with scaling exponent  $\beta \approx 1$ , as seen in panels A and C of figure 2. For the smaller crowders this effect is less pronounced, compare panels B and D. At later times the tracer motion starts to be affected by the confinement exerted by the outer reflecting membrane of the domain at  $r = R$ , and the MSD begins to saturate to a plateau. Concurrently the scaling exponent  $\beta(t)$  tends to zero.

The effect of the crowding fraction  $\phi$  on the MSD behaviour is illustrated in panels A and B of figure 2 for large and small crowders, respectively. For a tracer of unit size the larger crowders do not appear to create substantial obstruction for the simulated crowding fractions. Even at relatively large  $\phi$  values the MSD only marginally diminishes with increasing crowding fraction  $\phi$ , see panel A. In other words, small tracers always manage to manoeuvre around large void spaces remaining between large crowders.

In contrast, relatively small crowders at identical crowding fractions  $\phi$  yield severe reductions of the average diffusive tracer motion, as evidenced by panel B of figure 2. This observation is consistent with the dramatic differences of the spatial exploration patterns exhibited by the tracer in panels B of figure 1. The magnitude of the plateau of the MSD attained for larger  $\phi$  values is much smaller than expected for an annulus without crowders, compare with equation (11) below. This fact is due to the intricate labyrinthine environment formed by the unit sized crowders for diffusion of a tracer of the same size. For small crowders the value of the scaling exponent  $\beta$  is reduced significantly and at much earlier times for larger crowding fractions  $\phi$ , see panels C and D of figure 2. These features obviously strongly depend on the specific quenched environment, in which the tracer motion occurs, resulting in a high degree of irreproducibility of the tracer diffusion for different realisations of the disorder. This is also quantified in panel F of figure 2 (see below) and leads to substantially larger uncertainties in the local scaling exponent  $\beta(t)$  computed from the available MSD curves. The strong effect of small crowders on the MSD and the minor effect of the large crowders is our first main result.

We now turn to the analysis of the time averaged MSD obtained from averaging over  $10^4$  tracer trajectories for a single realisation of the crowder configuration. As shown in panel E of figure 2 for large crowders with  $R_c = 5$  and small crowding fractions  $\phi$  the spread of amplitudes of the time averaged MSD curves is quite small. At later times, when the tracer motion starts to be influenced by the outer boundary the average  $\langle \overline{\delta^2(\Delta)} \rangle$  approaches a plateau which has about twice the amplitude of the plateau value of the ensemble averaged MSD, see panel E in figure 2. Note that because of the relatively small domain size used in the simulations, the moderate trajectory lengths, and the presence of randomly distributed crowders this plateau is not as distinct as, for instance, for the deterministic, confined HDP, compare figure 4 in reference [70] and figure 8 in reference [71].

We recall that for the uncrowded case the long time (plateau) values of the ensemble and time averaged MSDs are related to the inner and outer radii in two dimensions as

$$\langle x^2 \rangle_{\text{st}} = \frac{1}{2} \langle \overline{\delta^2} \rangle_{\text{st}} \approx \frac{R^2 + a^2}{2}. \quad (11)$$

The occurrence of the factor 1/2 for the time averaged MSD is inherent to the very definition (6) [50, 51, 72]. The asymptote (11) is shown in panel E of figure 2 by the dotted line. The attainment of a plateau value of both ensemble and time averaged MSDs on a bounded domain is a typical feature of both ergodic processes such as Brownian motion and fractional Brownian motion as well as weakly non-ergodic processes, and is thus inherently different from the deviations from a plateau value in confining potentials [50, 72].

In contrast to these observations, for small crowders at high crowding fractions ( $\phi = 0.3$ ) the amplitude spread of the time averaged MSD curves for a particular distribution of crowders is quite pronounced, as shown in panel F of figure 2. The magnitude of the time averaged MSD is much smaller than that for larger crowders, compare the magnitude of the time averaged MSD in panels E and F of figure 2. In fact, time averaged MSD curves with very small magnitudes (below 1) resulted from almost immobile finite size tracers that were blocked by surrounding crowders. Moreover, the tracer only rarely reaches the outer cell membrane but mostly saturates at much lower values due to confinement by the crowders in a subdomain of our model cell. The MSD itself features a much more pronounced amplitude scatter for the same number  $N$  of traces used in the averaging. Because of the tracer localisation and the wide amplitude spread of the time averaged MSDs the mean time averaged MSD  $\langle \overline{\delta^2} \rangle$  has poor statistics and its relation to the ensemble averaged MSD prescribed by equation (11) is difficult to check. This behaviour of the time averaged MSD in homogeneous crowding environments is our second main result.

#### **4. Heterogeneous crowding case: ensemble and time averaged mean squared displacements**

How does a heterogeneous distribution of crowders affect the above results? An immediate effect of the heterogeneous distribution consists in very different properties for the in-out (from the nucleus surface to the membrane) and out-in (from the membrane to the nucleus) scenarios of the tracer diffusion. The average local density of crowders in the simulation domain (see panels C and D of figure 1) is generated according to equation (2) which naturally leads to a higher local diffusivity close to the nucleus that corresponds to the experimentally relevant diffusion of small proteins inside surface adhered eukaryotic cells [55, 73].

For the in-out diffusion from the nucleus to the cell periphery the tracers become trapped in progressively denser arrangements of crowders. At the same crowding fraction  $\phi$ , these trapping situations arise earlier in time for smaller crowders as compared to larger crowders, compare the panels C in figure 1. Similar to the homogeneous case the

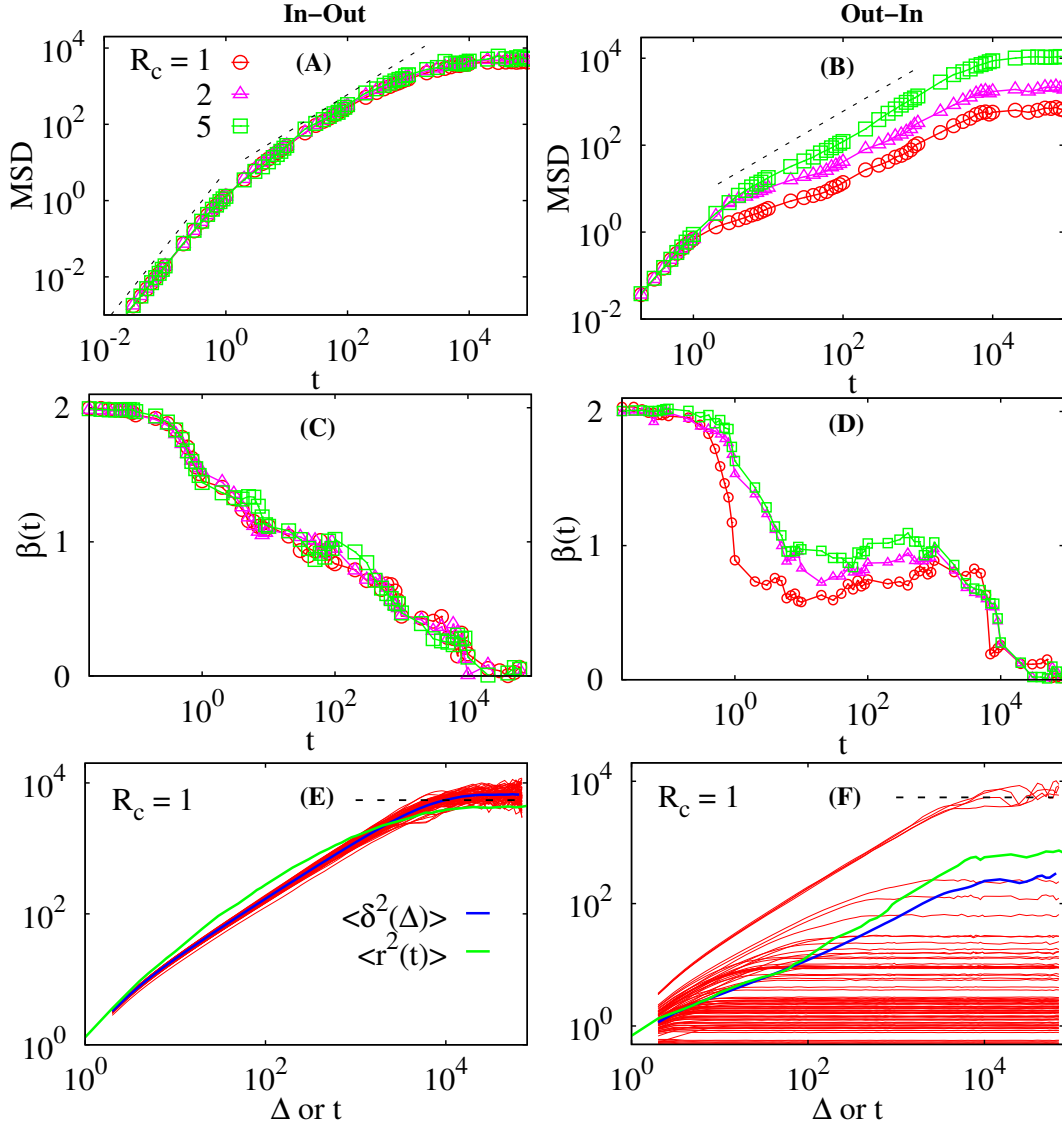


**Figure 3.** MSD, local scaling exponent  $\beta(t)$ , and time averaged MSD for tracer particles diffusing in heterogeneous crowder distributions of the form (2). The two columns correspond to the in-out and out-in tracer diffusion, that is, respectively, for the release of the tracer particle at the inner and outer radii of the model cell. The data for different crowder radii  $R_c$  are shown by different symbols in panels A-D. In panels A and B the dashed lines indicate the ballistic asymptote at short times and the linear Brownian regime at intermediate times. In panels E and F the long time plateau of the MSD for the uncrowded case given by the asymptote (11) is shown by the dashed line. Parameters:  $R = 100$ ,  $a = 30$ ,  $T = 10^5$ ,  $M = 100$ , and  $N = 100$ .

MSD starts ballistically, then reveals a linear Brownian regime, and finally saturates due to the confinement in the annulus. Concurrently, the local scaling exponent  $\beta(t)$  decreases continuously and finally vanishes when the MSD approaches a plateau, see panels A and C of figure 3. The spread of the time averaged MSD curves is relatively small and their long time plateau is again about twice of that of the ensemble averaged MSD for a particular crowder configuration, as expected from relation (11) and seen in panels E of figures 2 and 3. At intermediate times a stronger disparity between the ensemble and time averaged MSD is observed when compared to the homogeneous case, as shown in panel E of figure 3. The scatter of the time averaged MSD curves decreases when longer trajectories (larger  $T$  values) are analysed (results not shown). This behaviour is expected and is realised for several ergodic and nearly ergodic processes [50, 51]. The magnitude of the amplitude scatter of the time averaged MSDs in panels E of figures 2 and 3 is similar to that of Brownian motion [50, 52, 53].

In the opposite case of out-in diffusion (panel D of figure 1) we observe that for relatively high crowding fractions of small crowdors a finite size tracer often cannot even leave the vicinity of the boundary, giving rise to prolonged trapping events in this confined area. This leads to a large proportion of low amplitude, nearly constant time averaged MSD curves, as seen in panel F of figure 3. The magnitude of the mean time averaged  $\langle \delta^2(\Delta) \rangle$  is in many cases dominated by several successful fast translocation events of tracers from the cell membrane to the nucleus. In the long time limit equation (11) is thus not valid in this situation. The tracer localisation and the dominance of one or few extreme tracer trajectories in the mean value  $\langle \delta^2(\Delta) \rangle$  is also a rather common feature of stochastic processes in the presence of well pronounced traps as well as in ageing stochastic processes [50, 74]. The distinctly different behaviour between out-in and in-out diffusion in our heterogeneous crowder system is the third main results of this study.

Since the crowding fraction in equation (2) grows from the nucleus towards the cell periphery, the in-out diffusion in such heterogeneous crowdors distribution is expected to be subdiffusive [73]. In this scenario the tracers are progressively trapped closer to the cell periphery. Here, however, we observe the formation of a radial percolation in the circular domain: the tracers are not allowed to penetrate beyond some critical radius that features a particular critical density of crowdors, an effect that is crucially related to the finite size of both the crowdors and the tracer particle. Similar effects of local confinement are naturally observed for single particle trajectories of tracer diffusion in random percolation systems [69]. The initial period of the tracer diffusion that occurs in the region with low crowder density is naturally reproducible and leads to a small spread of the time averaged MSD curves, as shown in panel E of figure 3.

In contrast, for the out-in diffusion the tracer starts in the region of the highest concentration of crowdors and diffuses into regions containing less and less crowdors. The associated initial tracer localisation events give rise to stalling time averaged MSD curves with a very large spread, see panel F of figure 3. Early trapping in this scenario

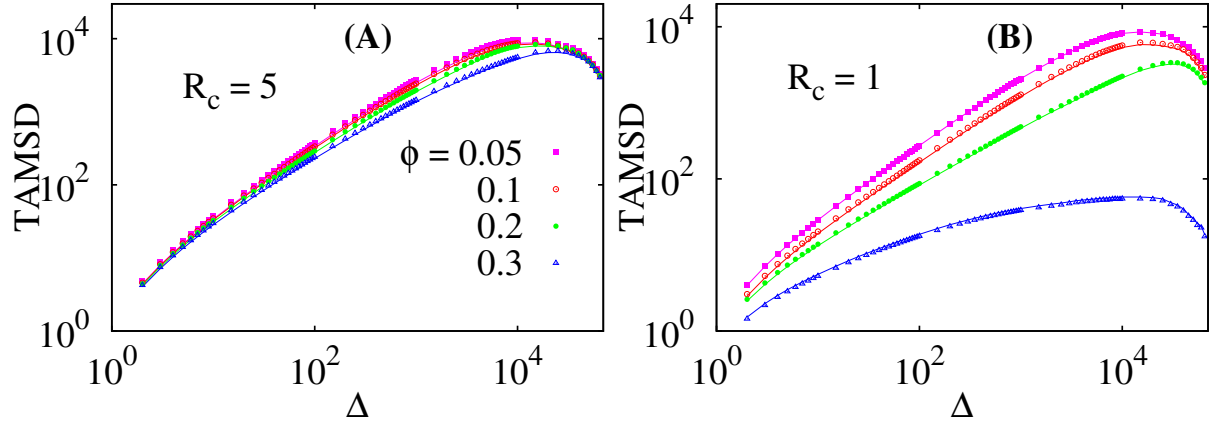


**Figure 4.** Time averaged MSD curves for trajectory based averaging only (solid lines;  $M = 1$ ,  $N = 10^4$ ) and for double averaging over tracer trajectories and realisations of the crowder distributions (symbols;  $M = 10^2$ ,  $N = 10^2$ ), computed for homogeneously distributed crowders. These curves can be compared to the results in panels E and F of Fig. 2. The crowder radius  $R_c$  and the crowding fraction  $\phi$  are indicated in the plots. Note that individual time averaged MSD curves are not shown, only the averages  $\langle \delta^2 \rangle$  and  $\langle \widetilde{\delta^2} \rangle$  are presented.

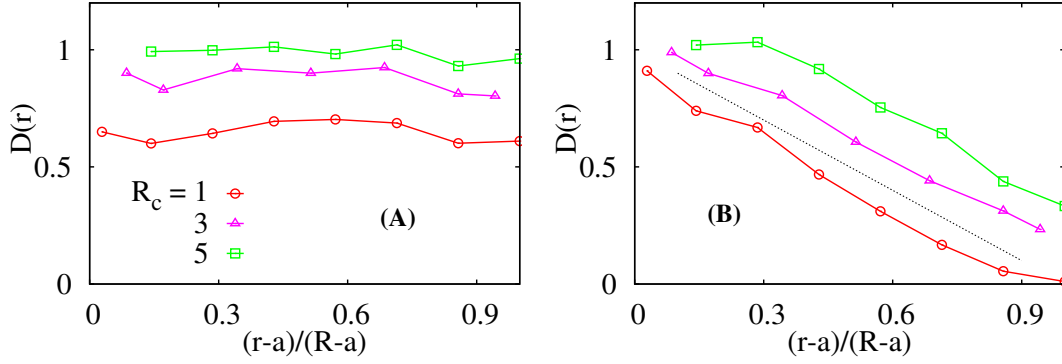
leads to the emergence of a longer plateau region in the corresponding time averaged MSD curve. The mean time averaged MSD computed over an ensemble of  $N$  trajectories is rather imprecise because of the dominance of few extreme events.

Figure 4 compares the averaging over  $N$  different tracer trajectories starting at random points at the nucleus boundary for a single crowder distribution and the double averaging that includes the average over  $M$  random realisations of crowders distribution. The time averaged MSDs for  $N = 100$  and  $M = 100$  are shown by symbols, while those for the case  $M = 1$  and  $N = 10^4$  are shown as solid lines. The two cases of homogeneously distributed crowders for large (panel A) and small (panel B) crowders are presented. We observe that the differences between the two averaging approaches are rather small: the single average over  $10^4$  trajectories and the double average over  $10^2$  trajectories and  $10^2$  crowder distributions yield very similar results.

We checked that for homogeneously distributed crowders the radial tracer diffusivity is approximately constant (panel A of figure 5), as it should be. In turn, for a heterogeneous distribution of crowders given by equation (2) the radial tracer diffusivity is a decreasing and nearly linear function of the distance from the nucleus (panel B of figure 5),

$$D(r) \approx D_0 \left( 1 - 0.78 \frac{r - a}{R - a} \right) + \text{const.} \quad (12)$$

The slope 0.78 is nearly independent on the crowder radius  $R_c$ . This linear dependency of the diffusivity seems to be a consequence of the linear increase of the crowders density as given by equation (2). This is our fourth main result.



**Figure 5.** Effective radial diffusivity of tracers for (A) homogeneous ( $\phi = 0.1$ ) and (B) heterogeneous ( $\phi(r)$ ) crowder distributions. Other parameters are the same as in figures 2 and 3, respectively, and the crowder radii  $R_c$  are as indicated. The dashed line in panel (B) represents the asymptote (12) without the last constant term.

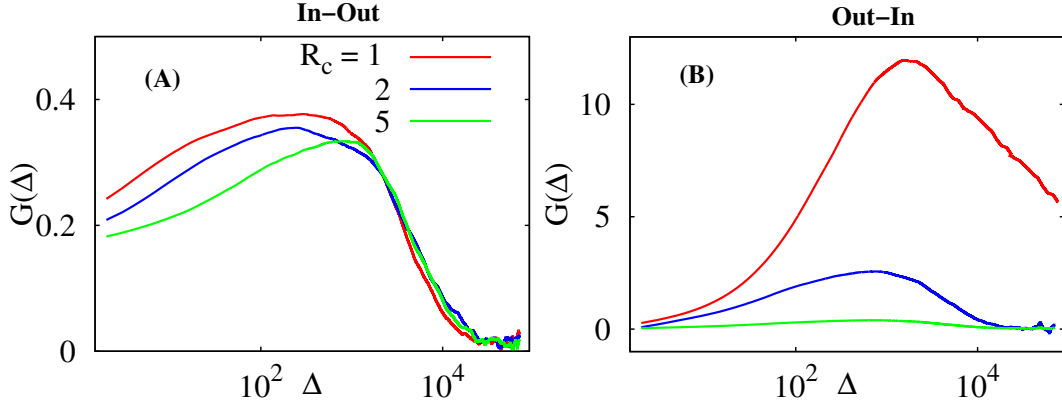


**Figure 6.** Non-Gaussianity parameter  $G(\Delta)$  (13) for in-out and out-in tracer diffusion. Parameters are the same as in figure 3 averaged over  $N = 10^4$  tracer trajectories for a single configuration of crowders ( $M = 1$ ).

## 5. Non-Gaussianity parameter and van Hove correlation function

Following reference [54] we now proceed to evaluate the experimentally relevant non-Gaussianity parameter for the tracer diffusion in our crowded environment. Similar to the ergodicity breaking parameter EB [50, 75] it contains the fourth order moment of the tracer time averaged MSD averaged over  $N$  realisations. Namely, in two dimensions we have [7, 76]

$$G(\Delta) = \frac{\langle \overline{\delta^4(\Delta)} \rangle}{2 \langle \overline{\delta^2(\Delta)} \rangle^2} - 1. \quad (13)$$

We find that for in-out diffusion the non-Gaussianity parameter assumes moderate values for shorter lag times  $\Delta$  while it becomes close to zero for longer lag times, as seen in panel A of figure 6. This is a typical long time behaviour of ergodic tracer

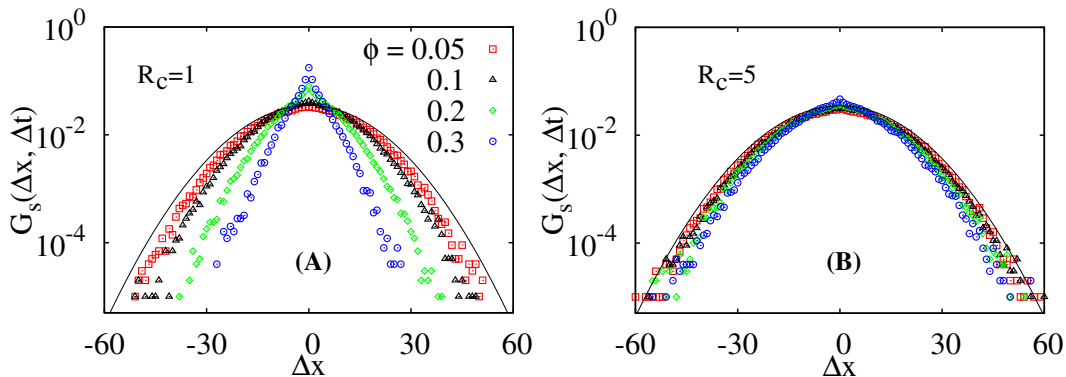


**Figure 7.** Van Hove correlation function for homogeneous crowder distribution and several crowding fractions  $\phi$ . Other parameters are the same as in figure 2. The solid line shows the approximately Gaussian function obtained from our simulations for a tracer restricted to an annulus without crowders. Panels A and B are for crowder radii  $R_c = 1$  and  $R_c = 5$ , respectively.

diffusion, compare figure 3a in reference [76]. Indeed, as we show in panel E of figure 3 in the long time limit the ensemble and time averaged MSDs differ simply by the above mentioned factor of 2 for heterogeneous crowder distributions. In contrast for out-in diffusion the non-Gaussianity parameter attains substantially larger values. This feature is likely due to the highly non-reproducible trajectories of the tracer motion and prolonged localisation events near the cell periphery in the region of high crowder concentration.

The trapping as well as the non-Gaussianity of the tracer diffusion can also be characterised by the van Hove correlation function  $G_s(\Delta x, \Delta t)$  describing the probability that a particle moves a distance  $\Delta x$  during time  $\Delta t$  [77, 78],

$$G_s(\Delta x, \Delta t) = \frac{1}{N} \sum_{i=1}^N \delta(x_i(\Delta t) - x_i(0) - \Delta x), \quad (14)$$

where  $N$  is the number of tracers used for averaging. For a system of hard spheres the van Hove correlation function simply corresponds to the diffusion propagator [79] governed by the diffusion equation.

Figure 7 shows the behaviour of the van Hove correlation function for tracer diffusion among homogeneously distributed crowders. We observe that for relatively large crowders the probability of trapping events of the tracer particle is quite low and the distribution of tracer displacements remains close to Gaussian for all crowding fractions studied, as it should (see panel B in figure 7). In contrast, for small crowders the non-Gaussianity of the van Hove function becomes quite pronounced, in particular for larger crowding fractions  $\phi$ , as demonstrated in panel A of figure 7. A faster decay of the tracer displacements at high crowding fractions  $\phi$  and for small crowders is a consequence of tracer caging by crowders and anomalously slow diffusion. The almost exponential distributions for high crowding fraction in panel A of figure 7 compare well with the experimentally measured step size distributions for polymer diffusion on nano-

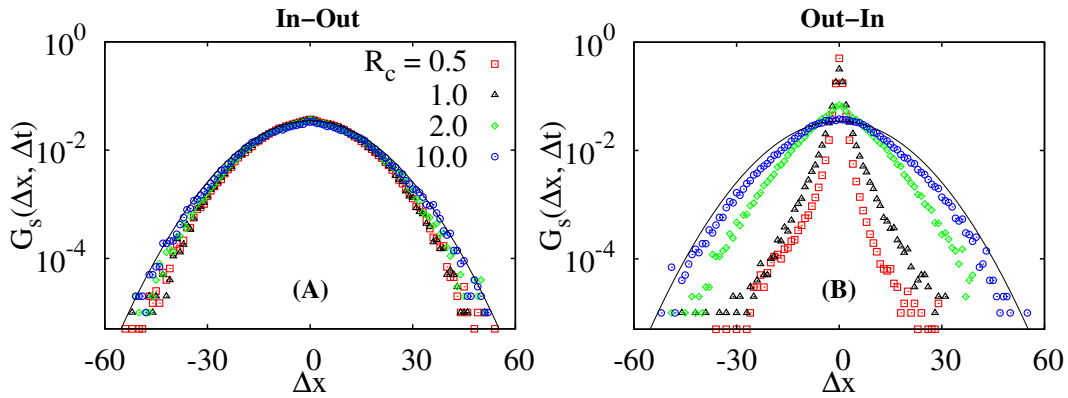


**Figure 8.** Van Hove correlation function for (A) in-out and (B) out-in diffusion plotted for several crowder radii  $R_c$  in the scenario of heterogeneous crowders distribution. The solid line shows the distribution of a tracer restricted to an annulus without crowders: it almost superimposes with the results for the largest crowders at  $R_c = 10$ . Other parameters are the same as in figure 3.

patterned surfaces presented in figure 4 of reference [80] as well as for liposome diffusion in nematic solutions of actin filaments in figure 3C of reference [81]. Heterogeneously structured environments for tracer diffusion cause a separation of particles into slow and fast populations (compare reference [82]), reflected in a cusp of the particle distribution near the origin and longer than Gaussian tails for large particle displacements.

For heterogeneous distributions of crowders the behaviour of the van Hove function is illustrated in figure 8. We observe that for in-out diffusion the distribution remains approximately Gaussian for all crowder radii  $R_c$  in our simulations. This corresponds to the rather small non-Gaussianity parameter and quite limited spread of the time averaged MSD curves in this situation. In contrast, for out-in diffusion among small crowders the probability distribution of tracer displacements becomes progressively non-Gaussian. It features a pronounced cusp near  $\Delta x = 0$  describing a prevalence of small displacements characteristic for subdiffusive processes in rather confined conditions. The detailed behaviour of the non-Gaussianity parameter and the van Hove correlation function represents the fifth main result of the present study.

## 6. Survival probability

First passage time statistics are important to describe cellular processes, for instance, to quantify the diffusion limit of reactions triggered by incoming, diffusing molecules. In the present cell model we focus on the first passage behaviour of particles arriving to the membrane from the nucleus surface (in-out case) or arriving to the nucleus surface from the cell boundary (out-in case). To examine this behaviour we consider the survival probability  $S(t)$  that a tracer started either at the inner nucleus or at the outer boundary, and does not attain a distance  $(a+r)$  away from the cell centre up to time  $t$ . The survival probability is directly related to the probability density of the first arrival time of the

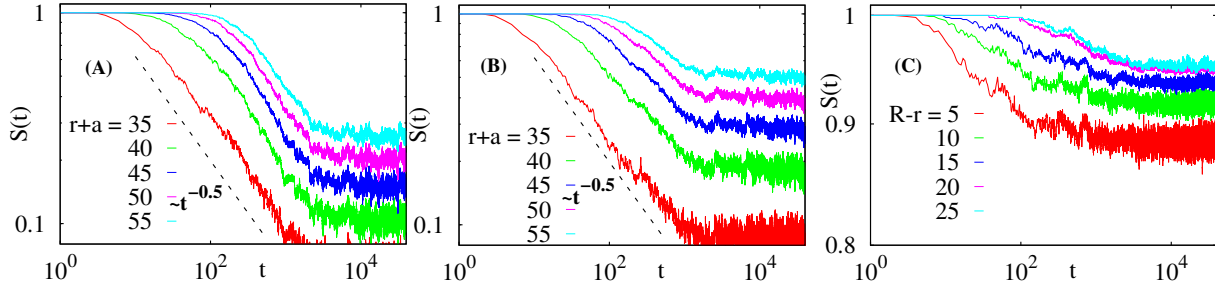


**Figure 9.** Survival probability  $S(t)$  for (A) homogeneous crowding (tracers are released near the nucleus), and for the heterogeneous crowding described by equation (2) for the cases of (B) in-out and (C) out-in diffusion. The asymptote  $S(t) \sim t^{-1/2}$  from (15) is shown in panels A and B. Different colours indicate  $S(t)$  for various distances  $(r+a)$  from the cell centre within which the tracers are counted. Neither the inner boundary at  $r = a$  nor the outer boundary at varying radius  $(a+r)$  are absorbing in the simulations. The model parameters for homogeneous and heterogeneous crowder configurations are the same as in figures 2 and 3, respectively.

tracer to that distance [83, 84].

Figure 9 shows the survival probability  $S(t)$  for homogeneously and heterogeneously distributed crowdors. For both homogeneous case and in-out diffusion we observe at intermediate times

$$S(t) \simeq t^{-1/2}. \quad (15)$$

In turn, for out-in diffusion  $S(t)$  has only a very weak dependence on the diffusion time  $t$ . As the distance  $(a+r)$  increases the survival probability starts to follow the scaling behaviour at later times, see figure 9. Similar scaling relations were obtained for subdiffusive HDPs with a diffusivity of the form  $D(r) = D_0 A / (A + r^2)$  for in-out diffusion of tracer particles [73]. We also simulated the tracer diffusion in the annulus without crowdors but with the effective radial diffusivity  $D(r)$  presented in figure 5. In these simulations, the same scaling law (15) for the survival probability was obtained, compare figures 9 and 10.

Figure 9 shows that the survival probability appears to saturate to finite values, instead of decaying to zero. The nonzero limiting value of the survival probability is related to the disorder averaging and should be equal to the fraction of crowdors configurations, in which the circle of radius  $a+r$  is not accessible for a finite size tracer. In fact, for such configurations the survival probability is 1, and it is then weighted by the fraction of these configurations. The behaviour of the survival probability is the sixth main result of this study.

## 7. Discussion and conclusions

The cytoplasm of living cells is a complex, superdense [1] mixture of various molecules of highly variable sizes, shapes, and surface properties, with often non-trivial spatial density distributions [55]. The passive diffusion of proteins such as transcription factors

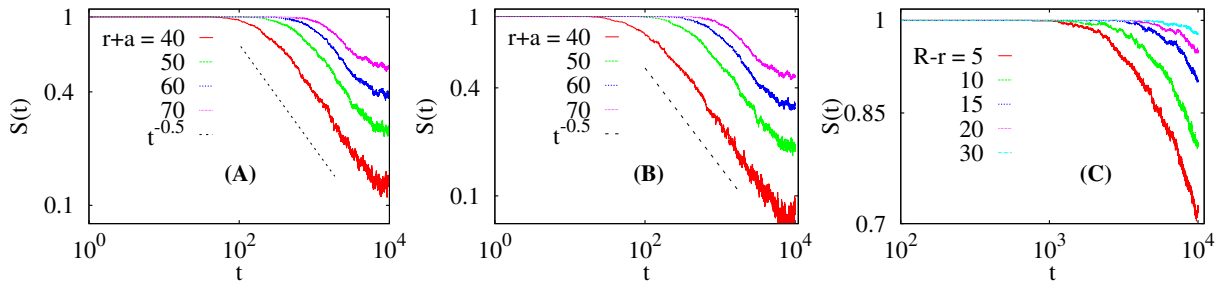


**Figure 10.** The same as in figure 9 but computed for the effective radial diffusivity  $D(r)$  from figure 5. The asymptote  $S(t) \sim t^{-1/2}$  is shown in panels A and B.

or enzymes, as well as other complex signalling molecules in living cells represents a vital ingredient in the cellular gene regulation and metabolism [85]. For instance, transcription factors that are taken up by the cell at its boundary need to diffuse to the nucleus, in which they will control the information transfer of certain genes. Conversely, viral components may be produced in the nucleus and are then transported by thermal diffusion (while larger parts are actively by molecular motors) to the cell membrane, where the assembly process of these viruses takes place [86]. The reverse process is, inter alia, relevant for the transport of internalised viruses to the nucleus [19, 87]. Recent experimental studies of the motion of relatively small green fluorescent proteins (GFPs) in both the cytoplasm and the nucleoplasm of living eukaryotic cells indeed demonstrate the existence of subdiffusion up to the millisecond range [12], concurrent to the existence of significant diffusivity gradients experienced by smaller proteins [55].

In earlier works, the spatial heterogeneity was often modelled through a space-dependent diffusivity. In particular, the implications of spatially heterogeneous diffusion processes (HDPs) with a prescribed gradient of the diffusion coefficient  $D(x)$  were studied on the basis of the overdamped Langevin equation for different functional forms of  $D(x)$  [88, 73, 70, 71]. These deterministic forms prescribe a systematic variation of the local particle diffusivity, similar to diffusivity maps in living cells [55, 56], and are thus inherently different from spatially and temporally *random* diffusivities [89, 90]. In particular, HDPs in a circular planar cell model with a radial diffusivity of the form  $D(r) = D_0 A / (A + r^2)$  exhibit radial subdiffusion with an anomalous diffusion exponent  $\beta = 1/2$ . In contrast to Brownian motion, the HDPs are weakly non-ergodic in the sense that time averages of physical observables such as the particle mean squared displacement do not converge to the corresponding ensemble averages even in the limit of long observation times [50].

In order to reveal the effect of molecular heterogeneity onto the intracellular transport, we performed extensive Langevin dynamics simulations of the motion of a passive tracer of a finite size in a two dimensional quenched disordered environment in which crowdiers are either homogeneously or heterogeneously distributed. The simulation domain was an annulus, which was limited by concentric inner and outer boundaries, representing the surface of the nucleus and the plasma membrane of the

cell. For varying crowding fraction and crowder size we quantified the motion of the tracer in the cell in terms of the diffusion profiles, the ensemble averaged MSD and the associated scaling exponent, as well as the time averaged MSD and the amplitude scatter observed for individual tracer trajectories. Finally, we also determined the degree of the non-Gaussian behaviour and the van Hove correlation function, as well as the survival statistics of the tracer.

Most theoretical and even numerical studies of the intracellular transport dealt with a point like tracer as studied, for instance, in reference [54]. In that case, one would expect that smaller crowders impede the tracer diffusion less, as the tracer can always pass through even small gaps between the crowders. In turn, the point tracer would have to navigate around larger crowders and thus be affected more severely. As we showed here the opposite effect occurs for a tracer of a finite size comparable to the size of the crowders. In this case many small crowders significantly hamper the spreading of the tracer as compared to larger crowders at the same crowding fraction  $\phi$ . Moreover, the van Hove correlation function acquires an exponential shape at higher crowding fractions and small crowders, whereas the van Hove correlation function is approximately Gaussian and quite insensitive to the crowding fraction for large crowders.

Concurrent to this effect we observe for larger, homogeneously distributed crowders an extended Brownian regime of the ensemble averaged MSD, whose magnitude is almost independent of the crowding fraction within the investigated range. The time averaged MSD in this case is also highly reproducible. For smaller crowders, however, anomalous diffusion effects in the ensemble averaged MSD occur and become more severe as  $\phi$  increases. Additionally, individual time averaged MSD curves demonstrate the early immobilisation of the tracer particles in the quenched landscape, corresponding to the crossing of a local percolation threshold for the tracer motion. In summary, when the tracer and crowder sizes are comparable, new dynamical features emerge as compared to conventional models with point like tracers.

Similar effects were observed for heterogeneously distributed crowders. Due to the deterministic gradient of the crowder distribution, two scenarios of in-out and out-in diffusion were distinguished depending on the location in which the tracer particle was released: either at the nucleus envelope or at the cell boundary. The in-out case resembles in many aspects the homogeneous case: the spread of the time averaged MSD is small, the van Hove correlation function is close to Gaussian and weakly depends on the crowder size, and the survival probability exhibits the characteristic square root decay at intermediate times. In contrast, the out-in case is marked by a highly non-Gaussian diffusion of the tracer: high values of the non-Gaussianity parameter and a pronounced cusp in the van Hove correlation function near  $\Delta x = 0$  reveal a prevalence of small displacements. This is characteristic for subdiffusive processes. Concurrently, the survival probability exhibits a very slow decay and tends to saturate at large values reflecting the dominating fraction of crowder configurations that block the tracer near the release point at the cell periphery. As a consequence, the computed averages over tracer trajectories are dominated by few successful translocation events.

In summary, our study revealed several important features for the tracer motion in a quenched disordered landscape, and is therefore also of interest from a purely statistical mechanical point of view. Possible applications of our results in the fields of biological or soft matter physics concern the diffusion of tracer particles or globular proteins in the heterogeneously crowded cytoplasmic fluid of surface adhering (flat) cells.

In order to focus on the effects of the finite size of the tracer particle and heterogeneous distributions of crowders, some other biologically relevant features of living cells were ignored. We investigated the effect of immobile crowders. On the time scale of the motion of many passive tracers architectural elements of the cell such as parts of the cytoskeleton or organelles may indeed be viewed immobile. Even large lipids or insulin granules are almost localised on such time scales [16, 18]. However, the motion of small crowders may be relevant as the effects such as the complete blocking of the tracer motion will be impeded. As shown recently the major effect of small mobile crowders is the increase of the effective viscosity experienced by the tracer particle [59]. In the present study we also neglected hydrodynamic interactions between the tracer and the crowders [91] which may affect the long time behaviour of the system. The slow,  $1/r$  decay of these hydrodynamic coupling forces implies that a diffusing particle is impacted by crowders from a finite distance that helps avoiding to collide with the crowders. Altering local pathways hydrodynamic forces may thus modify the diffusion statistics. Accounting for these interactions presents an interesting perspective. Other extensions of the current model include polydisperse static or dynamic crowders [92, 93], cylindrical domains mimicking typical bacterial shapes [45], specific tracer-crowders interactions [45, 54], three dimensional simulations, variable tracer size, and soft polymeric crowders [94].

## Acknowledgments

We acknowledge funding from the Academy of Finland (Suomen Akatemia, Finland Distinguished Professorship to RM), the Deutsche Forschungsgemeinschaft (Grant to AGC), and the French National Research Agency (Grant ANR-13-JSV5-0006-01 to DSG).

## References

- [1] I. Golding and E. C. Cox, *Phys. Rev. Lett.* **96**, 098102 (2006).
- [2] S. B. Zimmerman and S. O. Trach, *J. Mol. Biol.* **222**, 599 (1991).
- [3] S. B. Zimmerman and A. P. Minton, *Annu. Rev. Biophys. Biomol. Struct.* **22**, 27 (1993).
- [4] H. X. Zhou, *J. Mol. Recognit.* **17**, 368 (2004).
- [5] H. X. Zhou, G. Rivas, and A. P. Minton, *Annu. Rev. Biophys.* **37**, 375 (2008).
- [6] S. R. McGuffee and A. H. Elcock, *PLoS Comput. Biol.* **6**, e1000694 (2010).
- [7] F. Höfling and T. Franosch, *Rep. Progr. Phys.* **76**, 046602 (2013).
- [8] J.-P. Bouchaud and A. Georges, *Phys. Rep.* **195**, 127 (1990).
- [9] R. Metzler and J. Klafter, *Phys. Rep.* **339**, 1 (2000); *J. Phys. A* **37**, R161 (2004); E. Barkai, *Phys. Rev. E* **63**, 046118 (2001).

- [10] E. Barkai, Y. Garini, and R. Metzler, *Phys. Today* **65**(8), 29 (2012).
- [11] D. S. Banks and C. Fradin, *Biophys. J.* **89**, 2960 (2005).
- [12] C. Di Rienzo, V. Piazza, E. Gratton, F. Beltram, and F. Cardarelli, *Nature Comm.* **5**, 5891 (2014).
- [13] M. Weiss, M. Elsner, F. Kartberg, and T. Nilsson, *Biophys. J.* **87**, 3518 (2004).
- [14] S. C. Weber, A. J. Spakowitz, and J. A. Theriot, *Phys. Rev. Lett.* **104**, 238102 (2010).
- [15] I. Bronstein, Y. Israel, E. Kepten, S. Mai, Y. Shav-Tal, E. Barkai, and Y. Garini, *Phys. Rev. Lett.* **103**, 018102 (2009).
- [16] J.-H. Jeon, V. Tejedor, S. Burov, E. Barkai, C. Selhuber-Unkel, K. Berg-Sorensen, L. Oddershede, and R. Metzler, *Phys. Rev. Lett.* **106**, 048103 (2011).
- [17] E. Bertseva, D. S. Grebenkov, P. Schmidhauser, S. Gribkova, S. Jeney, and L. Forro, *Eur. Phys. J. E* **35**, 63 (2012).
- [18] S. M. A. Tabei, S. Burov, H. Y. Kim, A. Kuznetsov, T. Huynh, J. Jureller, L. H. Philipson, A. R. Dinner, and N. F. Scherer, *Proc. Natl. Acad. Sci. USA* **110**, 4911 (2013).
- [19] G. Seisenberger, M. U. Ried, T. Endress, H. Büning, M. Hallek, and C. Bräuchle, *Science* **294**, 1929 (2001).
- [20] J. Vercaammen, G. Martens, and Y. Engelborghs, *Springer Ser. Fluoresc.* **4**, 323 (2007).
- [21] W. Pan, L. Filobelo, N. D. Q. Pham, O. Galkin, V. V. Uzunova, and P. G. Vekilov, *Phys. Rev. Lett.* **102**, 058101 (2009).
- [22] J. Szymanski and M. Weiss, *Phys. Rev. Lett.* **103**, 038102 (2009).
- [23] D. Ernst, M. Hellmann, J. Köhler, and M. Weiss, *Soft Matter* **8**, 4886 (2012).
- [24] J.-H. Jeon, N. Leijnse, L. B. Oddershede, and R. Metzler, *New J. Phys.* **15**, 045011 (2013).
- [25] D. S. Grebenkov, M. Vahabi, E. Bertseva, L. Forro, and S. Jeney, *Phys. Rev. E* **88**, 040701(R) (2013).
- [26] D. S. Grebenkov and M. Vahabi, *Phys. Rev. E* **89**, 012130 (2014).
- [27] D. Ernst, J. Köhler, and M. Weiss, *Phys. Chem. Chem. Phys.* **16**, 7686 (2014).
- [28] C. H. Lee, A. J. Crosby, T. Emrick, and R. C. Hayward, *Macromol.* **47**, 741 (2014).
- [29] M. Weiss, H. Hashimoto, and T. Nilsson, *Biophys. J.* **84**, 4043 (2003).
- [30] A. V. Weigel, B. Simon, M. M. Tamkun and D. Krapf, *Proc. Natl. Acad. Sci. U. S. A.* **108**, 6438 (2011); D. Krapf, *Curr. Topics Membr.* **75**, 167 (2015).
- [31] C. Manzo, J. A. Torreno-Pina, P. Massignan, G. J. Lapeyre, Jr., M. Lewenstein, and M. F. Garcia Parajo, *Phys. Rev. X* **5**, 011021 (2015).
- [32] G. R. Kneller, K. Baczynski, and M. Pasienkewicz-Gierula, *J. Chem. Phys.* **135**, 141105 (2011).
- [33] J.-H. Jeon, H. Martinez-Seara Monne, M. Javanainen, and R. Metzler, *Phys. Rev. Lett.* **109**, 188103 (2012); M. Javanainen, H. Hammaren, L. Monticelli, J.-H. Jeon, R. Metzler, and I. Vattulainen, *Faraday Disc.* **161**, 397 (2013).
- [34] M. G. Wolf, H. Grubmüller, and G. Groenhof, *Biophys. J.* **107**, 76 (2014).
- [35] E. Yamamoto, T. Akimoto, M. Yasui, and K. Yasuoka, *Sci. Rep.* **4**, 4720 (2014).
- [36] A. Caspi, R. Granek, and M. Elbaum, *Phys. Rev. Lett.* **85**, 5655 (2000).
- [37] N. Gal and D. Weihs, *Phys. Rev. E* **81**, 020903(R) (2010)
- [38] D. Robert, T. H. Nguyen, F. Gallet, and C. Wilhelm, *PLoS ONE* **4**, e10046 (2010); compare the theoretical modelling of motor driven transport in viscoelastic, crowded media in I. Goychuk, V. O. Kharchenko, and R. Metzler, *PLoS ONE* **9**, e91700 (2014); *Phys. Chem. Chem. Phys.* **16**, 16524 (2014).
- [39] J. F. Reverey, J.-H. Jeon, H. Bao, M. Leippe, R. Metzler, and C. Selhuber-Unkel, *Sci. Rep.* **5**, 11690 (2015).
- [40] M. J. Saxton, *Biophys. J.* **70**, 1250 (1996).
- [41] F. Höfling, T. Franosch, and E. Frey, *Phys. Rev. Lett.* **96**, 165901 (2006).
- [42] X. L. Zhang, J. Hansing, R. R. Netz, and J. E. DeRouchey, *Biophys. J.* **108**, 530 (2015).
- [43] A. Godec, M. Bauer, and R. Metzler, *New J. Phys.* **16**, 092002 (2014).
- [44] H. Berry and H. Chate, *Phys. Rev. E* **89**, 022708 (2014).
- [45] F. Trovato and V. Tozzini, *Biophys. J.* **107**, 2579 (2014).

- [46] M. J. Saxton, *J. Phys. Chem. B* **118**, 12805 (2014).
- [47] L.-H. Cai, S. Panyukov, and M. Rubinstein, *Macromol.* **48**, 847 (2015).
- [48] I. M. Sokolov, *Soft Matter* **8**, 9043 (2012).
- [49] P. C. Bressloff and J. Newby, *Rev. Mod. Phys.* **85**, 135 (2013).
- [50] R. Metzler, J.-H. Jeon, A. G. Cherstvy, and E. Barkai, *Phys. Chem. Chem. Phys.* **16**, 24128 (2014).
- [51] D. S. Grebenkov, *Phys. Rev. E* **83**, 061117 (2011).
- [52] D. S. Grebenkov, *Phys. Rev. E* **84**, 031124 (2011).
- [53] A. Andreadov and D. S. Grebenkov, *J. Stat. Mech.* P07001 (2012).
- [54] S. K. Ghosh, A. G. Cherstvy, and R. Metzler, *Phys. Chem. Chem. Phys.* **17**, 472 (2015).
- [55] T. Kühn, T. O. Ihalainen, J. Hyvaluoma, N. Dross, S. F. Willman, J. Langowski, M. Vihinen-Ranta, and J. Timonen, *PLoS One* **6**, e22962 (2011).
- [56] B. P. English, V. Haurlyuk, A. Sanamrad, S. Tankov, N. H. Dekker, and J. Elf, *Proc. Natl. Acad. Sci. U.S.A.* **108**, E365 (2011).
- [57] A. P. Minton, *J. Biol. Chem.* **276**, 10577 (2001).
- [58] N. Dorsaz, C. De Michele, F. Piazza, P. De Los Rios, and G. Foffi, *Phys. Rev. Lett.* **105**, 120601 (2010).
- [59] J. Shin, A. G. Cherstvy, and R. Metzler, *Soft Matter* **11**, 472 (2015).
- [60] J. Shin, A. G. Cherstvy, and R. Metzler, *ACS Macro Lett.* **4**, 202 (2015).
- [61] H. Kang, P. A. Pincus, C. Hyeon, and D. Thirumalai, *Phys. Rev. Lett.* **114**, 068303 (2015).
- [62] J. Kim, C. Jeon, H. Jeong, Y. Jung, and B. Y. Ha, *Soft Matter* **11**, 1877 (2015).
- [63] J. D. Weeks, D. Chandler and H. C. Andersen, *J. Chem. Phys.* **54**, 5237 (1971).
- [64] I. Dukovski and M. Muthukumar, *J. Chem. Phys.* **118**, 6648 (2003).
- [65] C. Forrey and M. Muthukumar, *Biophys. J.* **91**, 25-41 (2006).
- [66] Y. Chen and K. Luo, *J. Chem. Phys.* **138**, 204903 (2013).
- [67] Y. M. Wang, R. H. Austin, and E. C. Cox, *Phys. Rev. Lett.* **97**, 048302 (2006).
- [68] A. Godec, A. V. Chechkin, E. Barkai, H. Kantz, and R. Metzler, *J. Phys. A* **47**, 492002 (2014).
- [69] Y. Mardoukhi, J.-H. Jeon, and R. Metzler, unpublished.
- [70] A. G. Cherstvy, A. V. Chechkin, and R. Metzler, *J. Phys. A* **47**, 485002 (2014).
- [71] A. G. Cherstvy and R. Metzler, *J. Stat. Mechan.* P05010 (2015).
- [72] J.-H. Jeon and R. Metzler, *Phys. Rev. E* **85**, 021147 (2012); S. Burov, R. Metzler, and E. Barkai, *Proc. Natl. Acad. Sci. USA* **107**, 13228 (2010).
- [73] A. G. Cherstvy, A. V. Chechkin, and R. Metzler, *Soft Matter* **10**, 1591 (2014).
- [74] J. Schulz, E. Barkai, and R. Metzler, *Phys. Rev. Lett.* **110**, 020602 (2013); *Phys. Rev. X* **4**, 011028 (2014).
- [75] Y. He, S. Burov, R. Metzler, and E. Barkai, *Phys. Rev. Lett.* **101**, 058101 (2008); S. M. Rytov, Yu. A. Kravtsov, and V. I. Tatarskii, *Principles of statistical radiophysics 1: elements of random process theory* (Springer, Heidelberg, 1987).
- [76] Y. Han, A. M. Alsayed, M. Nobili, J. Zhang, T. C. Lubensky, and A. G. Yodh, *Nature* **314**, 626 (2006).
- [77] M. J. Skaug, J. N. Mabry, and D. K. Schwartz, *J. Am. Chem. Soc.* **136**, 1327 (2014).
- [78] M. G. Del Popolo and G. A. Voth, *J. Phys. Chem. B* **108**, 1744 (2004).
- [79] P. Hopkins, A. Fortini, A. J. Archer, and M. Schmidt, *J. Chem. Phys.* **133**, 224505 (2010)
- [80] D. Wang, C. He, M. P. Stoykovich, and D. K. Schwartz, *ACS Nano* **9**, 1656 (2015).
- [81] B. Wang, J. Kuo, S. C. Bae, and S. Granick, *Nature Mater.* **11**, 481 (2012).
- [82] A. G. Cherstvy and R. Metzler, *Phys. Chem. Chem. Phys.* **15**, 20220 (2013).
- [83] S. Redner, *A Guide to First Passage Processes*, (Cambridge University Press, Cambridge, 2001).
- [84] *First-Passage Phenomena and Their Applications*, edited by R. Metzler, G. Oshanin, S. Redner (World Scientific, Singapore, 2014).
- [85] E. F. Koslover, M. A. Diaz de la Rosa, and A. J. Spakowitz, *Biophys. J.* **101**, 856 (2011); O. Bénichou, C. Chevalier, B. Meyer, and R. Voituriez, *Phys. Rev. Lett.* **106**, 038102 (2011); M. Bauer and R. Metzler, *PLoS ONE* **8**, e53956 (2013); crowding effects on the DNA may further

- influence the regulation process: G. Li, O. G. Berg, and J. Elf, *Nature Phys.* **5**, 294 (2009); C. Brackley, M. Cates, and D. Marenduzzo, *Phys. Rev. Lett.* **111**, 108101 (2013); M. Bauer, E. S. Rasmussen, M. A. Lomholt, and R. Metzler, *Sci. Rep.* **5**, 10072 (2015).
- [86] A. Zlotnick, personal communication, 2013.
- [87] A. Godec and R. Metzler, *Phys. Rev. E* **92**, 010701(R) (2015).
- [88] A. G. Cherstvy, A. V. Chechkin, and R. Metzler, *New J. Phys.* **15**, 083039 (2013). A. G. Cherstvy and R. Metzler, *Phys. Rev. E* **90**, 012134 (2014).
- [89] M. V. Chubynsky and G. W. Slater, *Phys. Rev. Lett.* **113**, 098302 (2014).
- [90] P. Massignan, C. Manzo, J. A. Torreno-Pina, M. F. Garca-Parajo, M. Lewenstein and G. L. Lapeyre, Jr., *Phys. Rev. Lett.* **112**, 150603 (2014).
- [91] D. Sarkar, S. Thakur, Y. G. Taoand, and R. Kapral, *Soft Matter* **10**, 9577 (2014).
- [92] V. Baranau and U. Tallarek, *Soft Matter* **10**, 3826 (2014).
- [93] D. Shah, A. L. Tan, V. Ramakrishnan, J. Jiang, and R. Rajagopalan, *J. Chem. Phys.* **134**, 064704 (2011).
- [94] J. Shin, A. G. Cherstvy, and R. Metzler, arXiv:1507.01176